energies

MDPI

Article

Numerical Modelling of Steam Superheaters in Supercritical Boilers

Katarzyna Węglarz [1], Dawid Taler [1], Jan Taler [2,*] and Mateusz Marcinkowski [1,*]

[1] Department of Thermal Processes, Air Protection and Waste Utilisation, Faculty of Environmental Engineering and Energy, Cracow University of Technology, ul. Warszawska 24, 31-155 Cracow, Poland
[2] Department of Energy, Faculty of Environmental Engineering and Energy, Cracow University of Technology, al. Jana Pawła II 37, 31-864 Cracow, Poland
* Correspondence: jtaler@pk.edu.pl (J.T.); mateusz.marcinkowski@pk.edu.pl (M.M.)

Abstract: This paper presents a numerical model of a four-pass supercritical steam superheater with a complex flow system. The specific heat of steam is a function of temperature and pressure, and the specific heat of flue gas is a function of temperature. Pressure and temperature changes along the length of the tubes were also determined. The modified Churchill equation was used to calculate the steam-side friction factor of Darcy–Weisbach. The flue gas temperature variations behind the individual superheater tube rows were calculated. The steam and wall temperature distributions were determined in each tube row along its length. Knowing the temperature of the tube walls and the steam along the flow direction enables the selection of the correct steel grade for the tubes. Thanks to this advantage of the proposed method, the investment can be reduced in superheater construction without the danger of overheating the tube material. The results of the superheater simulation were compared with the results of measurements on the actual object. The proposed numerical method can find application in steam superheaters' design and performance calculations. It can also be used to monitor superheater operating parameters, which are difficult to measure due to the high flue gas temperature.

Keywords: live steam superheater; mathematical model; supercritical steam boiler; pressure distribution; wall temperature distribution

Citation: Węglarz, K.; Taler, D.; Taler, J.; Marcinkowski, M. Numerical Modelling of Steam Superheaters in Supercritical Boilers. *Energies* **2023**, *16*, 2615. https://doi.org/10.3390/en16062615

Academic Editor: Gabriela Huminic

Received: 10 February 2023
Revised: 3 March 2023
Accepted: 8 March 2023
Published: 10 March 2023

1. Introduction

Steam superheaters in subcritical and supercritical boilers are used to increase the efficiency of electricity generation in steam power plants. The calculation and testing of superheaters in steam boilers receive significant attention. The interest in superheaters is because of the high temperature of superheater tubes and their high failure rate. More than 40% of emergency boiler shutdowns result from superheater tube failures. The ash fouling of superheater tubes causes severe difficulties in operating steam boilers. In addition to significantly reducing the heat flow rates exchanged between the flue gas and steam, ash deposits cause superheater tubes' corrosion. For this reason, many articles in the current literature address hydraulic, aerodynamic, thermal, and strength calculations. Examples of steam superheater failures and their causes are discussed extensively by French [1]. Pronobis [2] detailed superheater tubes' erosion and ash fouling processes. The book [2] contains rich experimental data on ash erosion of superheater tubes from the tests carried out on existing facilities and laboratory stands.

The literature on mathematical modelling and automatic control of supercritical power plants is extensive. The high interest in supercritical blocks is attributed to the large capacities of the power plants currently under construction and the greater efficiency of supercritical units. A very good review of the literature on the modelling and control of supercritical and ultra-supercritical steam power plants is presented by Omar [3]. Publications presenting mathematical models of supercritical fossil-fuel-fired power plants based

on thermal-flow process modelling are discussed. Models based on the laws of physics are more suitable for modelling significant power plant load changes and emergency conditions than the empirical-data-based models developed without any physical considerations. The authors highlight that the start-up optimisation process of a supercritical power plant has not been widely studied and appears to be an upcoming research proposal [3].

A mathematical model of a supercritical boiler for simulating its transient operation was presented by K. Hedrick et al. in [4]. Boiler load change from 100% to 60% was simulated, considering the change of boiler operation from subcritical to supercritical pressure. The boiler model was validated using measurements taken at an existing plant facility.

Haddad and Mohamed [5] presented three modelling procedures for a once-through supercritical power unit. The first mathematical model of a 600 MW power unit is based on the conservation equations of mass, momentum, and energy, the second uses a linearised state–space model, and the third uses artificial neural networks. All three approaches were compared against each other.

Young et al. [6] studied heat transfer at supercritical pressure with water flowing in a pipe. The pipe was heated at the outer surface. The heat flux varied from 100 to 1200 kW/m^2. The water flow regime varied from subcritical to supercritical. Heat transfer correlations were proposed to calculate the heat transfer coefficient at the pipe's inner surface.

The method of determining the tube temperature and the thickness of the inner oxide scales at the superheater tubes was developed by Sun and Yan [7]. The thickness of the oxide scale layer can be determined along the tube's length as a function of time using the method proposed in [7]. Local overheating of the tube walls in superheaters is a cause of tube creep and tube failure. Li et al. [8] developed an online procedure for superheater tube monitoring based on Computational Fluid Dynamics (CFD) modelling and flue gas side measurements. The purpose of the system is to prevent overheating of the tube material. Oxide deposits on the inner surfaces of superheater tubes pose a significant threat to the durability of superheaters. Due to the increase in the operating temperature of the tube walls, there is a danger of the tube material overheating. In addition, stripping of the oxide layer from the pipe surfaces poses a severe threat to the life of the steam turbine. The impact of temperature on the oxide spallation intensity in ferritic–martensitic superheater tubes was studied by Qi et al. in [9].

Analyses made by Balint et al. [10] provide new insights into the melting and ageing behaviour of ash deposits, which play an essential role in the corrosion of superheater tubes. Cross sections of ash deposit layers on superheater tubes were analysed using scanning electron microscopy and energy-dispersive X-ray analysis. Failure analysis of the superheater tubes was carried out by Liu [11] in a boiler fired with black liquor. Creep and thermal fatigue were identified as the main cause of superheater failure. The fractographic analysis identified two cracks at the heat-affected zone of the weld. The cracks initiated on the fireside surface of the tube and moved toward the inner surface of the tube. One of the analysed cracks propagated through the tube wall and caused damaging the superheater tube and steam flow out of it. An important phenomenon that significantly affects the life of superheater tubes is the uneven temperature distribution across the width of superheater platens. The non-uniformity of the mass flow rates in the individual tubes causes temperature differences in parallel tubes of the platens. In addition, the differences in the flue gas temperature in the duct cross-section can cause temperature differences across the width of the superheater. The steam temperature non-uniformity in an L-shaped platen superheater in a supercritical 600 MW circulating fluidised bed boiler (CFB) was studied by Ma et al. [12]. Thermal flow calculations of the entire steam boiler with natural circulation are presented by Hossain et al. in [13]. The paper [13] is particularly interesting to boiler designers because it provides thermal calculations of the entire boiler. The effectiveness–number of transfer units (ε-NTU) method was used for superheater performance calculations, and the logarithmic mean temperature difference (LMTD) method for design calculations. Determining the superheater tube temperatures was not at the aim

of this work. Steam superheaters in pulverised and fluidised bed boilers often fail due to the excessive temperature of the tube material. The computational determination of the maximum wall temperature of superheater tubes is very difficult due to the complexity of thermal and flow processes occurring in the boiler. Often, the only reliable method of determining the cause of superheater tube failure is to measure continuously the tube wall temperature during boiler operation. A new technique for measuring the tube wall temperature in CFB boilers was developed by Yao et al. [14].

CFD methods are widely used in the analysis of flow and thermal phenomena occurring in pulverised coal-fired steam boilers or fluidised bed boilers. A three-dimensional (3D) mathematical model of combustion and heat transfer on the flue gas side and a one-dimensional mathematical model of heat transfer in the tubes of a hanging radiant superheater were developed by Laubscher and Rousseau [15]. The steady-state and transient flow and thermal phenomena in subcritical boiler steam superheaters were analysed by Granda et al. [16] using CFD modelling. Thermal and flow calculation results of the second-stage steam superheater located at the combustion chamber of the large-scale CFB boiler are presented by Madejski et al. [17].

A significant group of calculation methods for steam superheaters are analytical and semi-analytical methods. Usually, a method using the LMTD between the flue gas and steam is used. The LMTD procedure is applied, for example, by Lokshin et al. [18] in the standard method of hydraulic design for power boilers. In addition, Kagan et al. [19] utilised the LMTD method for the thermal calculating of superheaters. The LMTD method makes it possible to calculate the heat exchange area of the superheater without considering the temperature of the tubes. Unlike low-temperature heat exchangers, a significant difficulty in calculating steam superheaters is the determination of the radiation heat transfer coefficient (HTC) on the flue gas side. An alternative method to [19] for calculating the radiation and convection HTCs on the flue gas side was proposed by Olenev [20]. A simple formula for calculating the radiation HTC at the superheater tube surface based on the P1 method of radiation heat transfer analysis in gases was presented by Taler and Taler [21].

In large steam boilers with supercritical steam pressure, the wall thickness of superheater tubes is greater than in subcritical boilers. In addition, the steam temperature in modern steam superheaters is approximately 600 °C. In order not to increase excessively the thickness of tube walls and to ensure their resistance to high-temperature corrosion, high-alloy steels are used for superheater tubes. For steam temperatures not exceeding 600 °C, ferritic–martensitic steels are used, and at higher temperatures, austenitic steels are applied. Each superheater pass is made of a different steel grade adjusted to the operating temperature to reduce investment costs. It is necessary to know the temperature variation of steam along the flow path to select the suitable grade of steel for a given superheater pass. A hybrid numerical–analytical method for calculating cross-flow tube heat exchangers was presented by Taler et al. [22]. The method also makes it possible to calculate quickly the temperature distribution of flue gas, steam, and tube walls, taking into account the temperature-dependent thermal properties of both fluids and the tube material. Flue gas and steam temperature are expressed in each finite volume by exact analytical formulas. A non-iterative calculation procedure for tube cross-flow heat exchangers was also developed by Węglarz et al. [23]. The temperature of steam and flue gas at the outlet of the finite volume is calculated using analytical expressions. The calculation formulas are straightforward. Computer calculation times are short even with the more significant number of finite volumes required in this method compared with the method presented in the work [22]. Both semi-analytical methods [22,23] are suitable for calculating cross-co-current and cross-counter-current superheaters with complex flow arrangements.

Most of the analytical methods used to calculate tubular heat exchangers, i.e., the LMTD, ε-NTU, and P-NTU methods, assume a constant specific heat throughout the heat exchanger. It should be added here that the ε-NTU method is also used in commercial CFD

programs to calculate the average temperature of both fluids at the outlet of tubular heat exchangers, including steam superheaters.

A review of the work published to date shows that there is a lack of uncomplicated yet accurate superheater models to determine local steam, flue gas, and tube wall temperatures. The aim of this article is to develop a new numerical model of a four-pass cross-counter flow live steam superheater. The calculation procedure accounts for temperature-dependent steam, flue gas, and tube material properties. Superheater calculations were carried out for a third-stage live steam superheater installed in a supercritical boiler. The mass capacity of the boiler was 645 kg/s. The results of calculations using the proposed model were validated against the measured temperatures of steam and flue gas at the superheater outlet. The developed method is simple and can be used to calculate superheaters and other cross-flow tubular heat exchangers with complicated flow systems. The advantage of the method is that it requires little effort to build a mathematical model of the heat exchanger and has a very short computer calculation time. Because of the short calculation time, the superheater model developed in this paper can be used for online monitoring of superheater operation. By using the model, steam and wall temperature distributions can be determined along the length of the superheater tubes, which would be difficult to measure directly due to the high flue gas temperatures.

2. A Mathematical Modelling Method for Tube Cross-Flow Heat Exchanger

The calculation of the temperature distribution of the two fluids in the heat exchanger will first be presented, and then the procedure for determining the pressure drop inside the tubes will be described.

2.1. Determination of the Temperature Distribution of Fluids

The method presented in [23] was used to simulate the third-stage steam superheater in a supercritical pressure boiler. The tubular heat exchanger was divided into finite volumes (Figure 1). Formulas were obtained for calculating the temperature of the fluid *a* and *w* at the outlet of the finite volume. The energy conservation equations for steam flowing through the tubes and flue gas flowing perpendicular to the tube axis were used to derive formulas for outlet temperatures of both fluids.

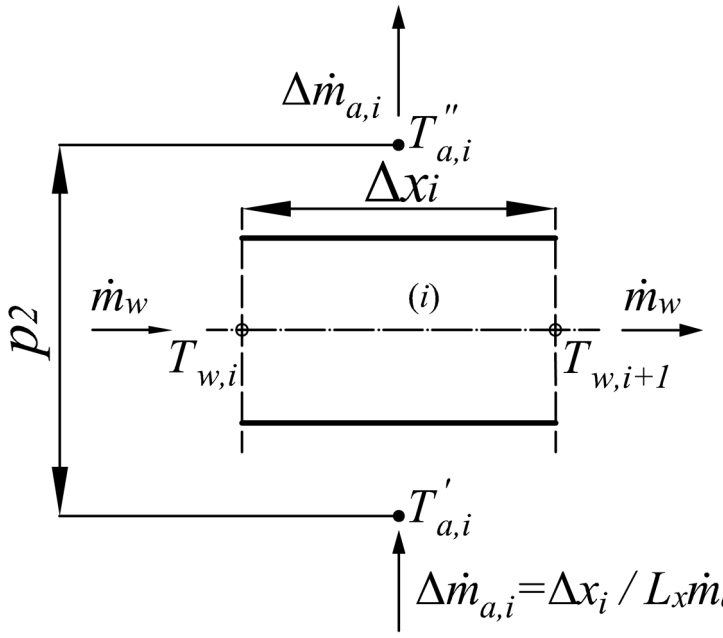

Figure 1. Diagram illustrating the calculation of the temperature of the fluid *w* flowing inside the tube and the temperature of the fluid *a* flowing transversely to the tube axis.

The symbols $T_{w,i}$ and T'_a in Figure 1 designate inlet temperatures of fluid w and a, and $T_{w,i+1}$ and T''_a are outlet temperatures of fluid w and a, respectively. The symbol $\Delta\dot{m}_{a,i} = \dot{m}_{a,i}\Delta x_i / L_x$ designates the mass flow rate of fluid a per a single finite volume of length Δx_i. The symbol $\dot{m}_w$ represents the mass flow rate of fluid w per a single tube. The p_2 symbol indicates the longitudinal tube spacing (pitch) in the heat exchanger.

If the inlet temperatures $T_{w,i}$ and T'_a are known, the temperature $T_{w,i+1}$ is calculated using the following expression:

$$T_{w,i+1} = \frac{2\frac{\Delta N_{a,i}}{\Delta N_{w,i}}\ T_{w,i}\ +\ \left(2T'_{a,i} - T_{w,\,i}\right)[1-\exp(-\Delta N_{a,i})]}{2\frac{\Delta N_{a,i}}{\Delta N_{w,i}}\ +\ [1-\exp(-\Delta N_{a,i})]},\ \ i = 1,\ldots,n \tag{1}$$

where $\Delta N_{a,i}$ and $\Delta N_{w,i}$ denote the number of heat transfer units (NTU) for fluid a and w, respectively.

The NTU values for the i-th finite volume are calculated as follows:

$$\Delta N_{a,i} = \frac{k_i\ \Delta\ A_{out,i}}{\Delta\dot{m}_{a,i}\ \overline{c}_{pa,\,i}} \tag{2}$$

$$\Delta N_{w,i} = \frac{k_i\ \Delta\ A_{out,i}}{\dot{m}_w\ \overline{c}_{pw,i}} \tag{3}$$

The overall heat transfer coefficient k_i refers to the external surface of the tube with an area of $\Delta\ A_{out,i} = \pi\ d_{out}\ \Delta\ x_i$, where the symbol d_{out} denotes the tube's outer diameter.

The mean specific heat capacities $\overline{c}_{pa,i}$ and $\overline{c}_{pw,i}$ are defined as follows:

$$\overline{c}_{pa,i} = \frac{c_{pa}(T'_a) + c_{pa}(T''_a)}{2} \tag{4}$$

$$\overline{c}_{pw,i} = \frac{c_{pw}(T_{w,i}) + c_{pw}(T_{w,i+1})}{2} \tag{5}$$

If the temperature $T_{w,i+1}$ and the temperature T'_a are known, the temperature $T_{w,i}$ is calculated using the following formula:

$$T_{w,i} = \frac{T_{w,i+1}\left\{2\frac{\Delta N_{a,i+1}}{\Delta N_{w,i+1}}\ +\ [1-\exp(-\Delta N_{a,i+1})]\right\}\ -\ 2T'_{a,i}[1-\exp(-\Delta N_{a,i+1})]}{2\frac{\Delta N_{a,i+1}}{\Delta N_{w,i+1}} - [1-\exp(-\Delta N_{a,i+1})]} \tag{6}$$

Formula (1) applies when the temperature of the fluid w is calculated in the direction of flow. Formula (6) applies when the temperature of the fluid w is calculated opposite to its flow direction.

If the temperatures $T_{w,i}$ and $T_{w,i+1}$ are known, then the temperature T''_a of the fluid a at the outlet of the finite volume is calculated from the formula:

$$T''_{a,i} = \overline{T}_{w,i} - \left(\overline{T}_{w,i} - T'_{a,i}\right)\ \exp(-\Delta N_{a,i}) \tag{7}$$

where the average fluid temperature w on the finite volume length $\Delta x_i = x_{i+1} - x_i$ is defined as

$$\overline{T}_{w,i} = \frac{T_{w,\,i} + T_{w,\,i+1}}{2} \tag{8}$$

In the case of a uniform tube division in one pass of length L into n finite volumes, the finite volume length is $\Delta x = L/n$. In order to avoid iteration, it is usually assumed $\overline{c}_{pa,i} = c_{pa}(T'_a)$, $\overline{c}_{pw,i} = c_{pw}(T_{w,i})$ for Equation (1) and $\overline{c}_{pa,i} = c_{pa}(T'_a)$ Equation (6).

Formulas (1), (6), and (7) apply to determine the outlet fluid temperatures of each finite volume. It should be noted that solving a system of algebraic equations is not necessary

when determining the node temperatures in all finite volumes. It is an essential advantage of the method used.

The temperature $T^j_{t,i}(r_{out})$ of the tube at the outer surface in the i-th finite volume in the j-th row is given by

$$T^j_{t,i}(r_{out}) = \overline{T}^j_{w,i} + \dot{q}^j_{out,i}\left(\frac{r_{out}}{r_{in}}\frac{1}{h^j_{w,i}} + \frac{r_{out}}{\lambda^j}\ln\frac{r_{out}}{r_{in}}\right) i = 1,\ldots,n,\ j = 1,\ldots,n_t \tag{9}$$

where the heat flux at the tube outer surface is given by the expression:

$$\dot{q}^j_{out,i} = k^j_i\left(\overline{T}^j{}_{a,i} - \overline{T}^j{}_{w,i}\right) = k^j_i\left(\overline{T}^j{}_{a,i} - \frac{T^j_{w,i} + T^j_{w,i+1}}{2}\right) \tag{10}$$

The overall HTC k^j_i referred to the tube outer surface is calculated as follows:

$$\frac{1}{k^j_i} = \frac{r_{out}}{r_{in}}\frac{1}{h^j_{w,i}} + \frac{r_{out}}{\lambda^j_i}\ln\frac{r_{out}}{r_{in}} + \frac{1}{h^j_{a,i}} \tag{11}$$

The following designations are used in Formulas (9)–(11): i and j—the number of finite volumes and the number of tube rows,

$\overline{T}^j_{w,i} = 0.5\left(T^j_{w,i} + T^j_{w,i+1}\right)$—mean temperature of the fluid w across the length Δx_i of the finite volume, °C,

$\dot{q}^j_{out,i}$—heat flux at the tube outer surface for the i-th finite volume and j-th tube row, W/m^2,

r_{in}, r_{out}—inner and outer tube diameters, m,

$h^j_{w,i}$—HTC at the inner surface of the tube (on the fluid side w), W/(m^2·K),

$h^j_{a,i}$—HTC at the outer surface of the tube (on the fluid side a), W/(m^2·K),

λ^j_i—tube material thermal conductivity for i-th finite volume in j-th tube row, W/(m·K),

n_t—number of tube rows in the heat exchanger.

The average flue gas temperature over the thickness of the j-th row of tubes in the i-th finite volume was calculated using the following formula:

$$\overline{T}^j{}_{a,i} = \int_0^1 T^j_{a,i}\left(y^+_j\right)\mathrm{d}y^+_j = \overline{T}^j_{w,i} + \frac{1}{\Delta N^j_{a,i}}\left[\left(T^j_{a,i}\right)' - \overline{T}^j_{w,i}\right]\left[1 - \exp\left(-\Delta N^j_{a,i}\right)\right] \tag{12}$$

The HTC at the tube's inner surface $h^j_{w,i}$ was calculated from the Dittus–Boelter formula [18,19]:

$$Nu_a = 0.021\mathrm{Re}^{0.8}\mathrm{Pr}^{0.4} \tag{13}$$

The HTC $h^j_{w,i}$ can be calculated more precisely using the simple correlations given by Taler [24] and Taler and Taler [25], the form of which depends on the value of the Prandtl number.

2.2. Determination of Pressure Distribution

The momentum conservation equation for steady one-dimensional fluid flow in a channel shown in Figure 2 is given by Taler [26]:

$$w\frac{\partial w}{\partial s} = -\frac{1}{\rho}\frac{\partial p_w}{\partial s} - g\,\sin\varphi - \frac{\xi}{d_h}\frac{w|w|}{2} \tag{14}$$

where

w—fluid velocity, m/s,

p_w—static pressure, Pa,

s—the coordinate passing through the centre of gravity of the duct cross-section, with the same direction as that of the velocity vector, m,
ρ—density of the fluid, kg/m^3,
g—acceleration of gravity, m/s^2,
φ—inclination angle of the duct axis to the horizontal plane, rad,
ξ—Darcy–Weisbach friction factor, -,
d_h—hydraulic diameter, m.

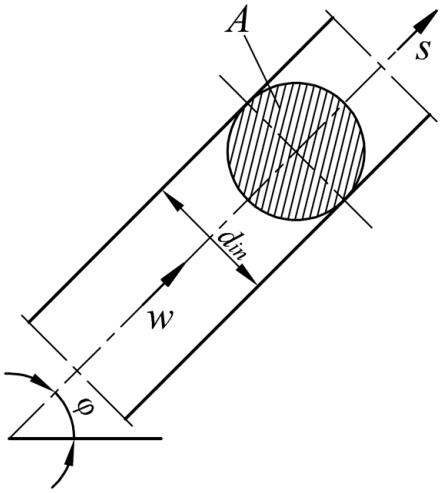

Figure 2. Steam flow through a superheater tube with the inner diameter d_{in} inclined to the horizontal plane at an angle φ.

In the component representing the friction pressure drop, the absolute value of the velocity is present to take into account the return of the velocity vector. It should be noted here that the pressure drop occurs in the direction of the flowing fluid. The momentum conservation Equation (14) can also be written as a function of the mass flow rate of the flowing fluid $\dot{m}$:

$$\frac{\partial}{\partial s}\left(\frac{\dot{m}^2}{\rho A}\right) = -A\left(\frac{\partial p_w}{\partial s} + \rho\, g\, \sin\varphi + \frac{\xi}{d_h}\,\frac{\dot{m}|\dot{m}|}{2\,\rho A^2}\right) \tag{15}$$

where A is the cross-sectional area of the channel, m^2.

Equation (14) can be written in the form:

$$-\quad \frac{\partial p_w}{\partial s} = \rho\left[w\frac{\partial w}{\partial s} + g\, \sin\varphi + \frac{\xi}{d_h}\frac{w|w|}{2}\right] \tag{16}$$

The first term in square brackets in Equation (16) represents the pressure drop due to the variation in the velocity of the flowing fluid, the second the gravitational pressure loss, and the third the pressure drop due to friction. Equation (16) was solved using the finite difference method. The differential Equation (16) was approximated using the finite difference method:

$$\frac{p_{w,i+1} - p_{w,i}}{\Delta s} = -\,\rho_i\left[w_i\frac{w_{i+1} - w_i}{\Delta s} + g\, \sin\varphi_i + \frac{\xi_i}{d_h}\frac{w_i|w_i|}{2}\right] \tag{17}$$

The subscript i refers to the inlet to the finite volume and index $(i + 1)$ to the outlet. The mean values of fluid density and flow velocity were assumed to be equal to the

corresponding values at the inlet to the finite volume. The pressure at the outlet of the finite volume determined from the solution of Equation (17) has the following form:

$$p_{w,i+1} = p_{w,i} - \rho_i \, \Delta s \left[w_i \frac{w_{i+1} - w_i}{\Delta s} + g \, \sin \varphi_i + \frac{\xi_i}{d_h} \frac{w_i |w_i|}{2} \right] \tag{18}$$

The fluid flow velocity w_i at the inlet to the i-th cell (finite volume) was calculated as follows:

$$w_i = \dot{m} / (\rho_i \, A_i) \tag{19}$$

It should be noted that in the steady state, $\dot{m}_i = \text{const}$.

Local pressure losses, such as pressure drops at bends, valves, and constrictions or expansions of the tube cross-section, are not included in the Equation (18).

Pressure drops at local resistances are usually taken into account at the boundary between two finite volumes. For example, for a modelled four-pass superheater, there are two 90° bends where steam flows from one pass to the other.

If the steam pressure $p_{w2,n+1}$ in the first tube row (in the fourth superheater pass) and the pressure $p_{w1,1}$ in the second tube row (the third superheater pass) are known at the finite volume nodes, the pressure drop across the two bends between the second and first tube row is given by the formula (Figure 3). After taking into account that the pressure $p_{w2,n+1}$ is known from the calculation of the second tube row (third pass), the pressure $p_{w1,1}$ at the inlet to the first tube row (fourth pass) is calculated:

$$p_{w2,n+1} - p_{w1,1} = \sum_{j=1}^{2} \zeta_j \frac{\rho_j \, w_j^2}{2} \tag{20}$$

where the symbol ζ_j denotes the pressure lost coefficient for a 90° bend.

Similarly, we proceed with the determination of the pressure drop at the bends occurring between each row.

The values of the coefficients ζ_j can be found for a number of elements in the work of Lokshin et al. [18] and in the handbook of Idelchik [27]. The friction factor ξ_i can be read from Moody's [28] diagram. In computer calculations, it is more convenient to use explicit relations to determine the friction factor in tubes with rough surfaces. The explicit Churchill formula modified by Rennels and Hudson [29] is very accurate for determining the friction factor:

$$\xi = \left[\left(\frac{64}{\text{Re}} \right)^{12} + \frac{1}{(A+B)^{3/2}} \right]^{1/12}, \; 500 < \text{Re} < 10^8 \tag{21}$$

where the coefficients A and B are given by

$$A = \left[0.8687 \, \ln \frac{1}{\frac{0.883 \, (\ln \, \text{Re})^{1.282}}{\text{Re}^{1.007}} + 0.27 \, \varepsilon - \frac{110 \, \varepsilon}{\text{Re}}} \right]^{16} \tag{22}$$

$$B = \left(\frac{13269}{\text{Re}} \right)^{16} \tag{23}$$

The symbol ε in Equation (22) designates relative roughness equal to $\varepsilon = R_a / d_{in}$, where the symbol R_a denotes the absolute roughness of the inner tube surface.

The method described above was applied to the determination of the steam and flue gas temperature distribution and pressure drop inside the tubes in a four-pass counter-flow superheater with supercritical steam pressure.

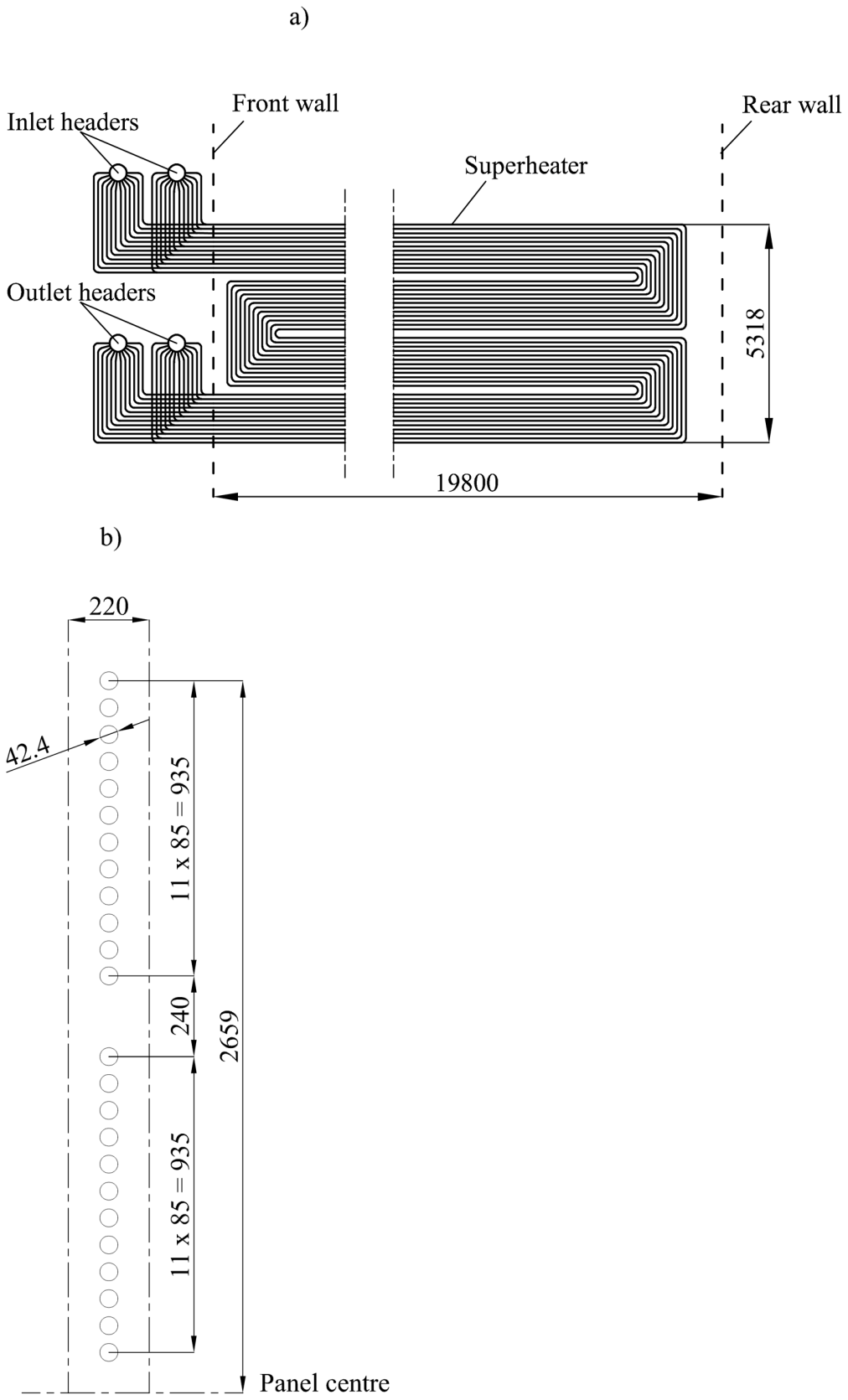

Figure 3. Four-pass live steam superheater; (**a**) side view of a single panel with four passes in which steam flows through 12 parallel tubes and (**b**) tube arrangement in half of a single panel. The numbers in the figure indicate the dimensions in millimetres.

3. Mathematical Model of Cross-Counter-Current Superheater with Four Passes

The modelled third stage of the live steam superheater consisted of 88 four-pass panels. A side view of a single panel is shown in Figure 3a. In a single panel (platen) with 4 passes, steam flowed parallel through 12 tubes. The height of a single panel was 5318 mm. There were $4 \times 12 = 48$ tubes (48 horizontal tube rows) per panel height. Considering that there were 88 panels in the superheater, the steam flowed parallel through $12 \times 88 = 1056$ tubes. The transverse spacing of the panels was $p_1 = 220$ mm, and the longitudinal tube spacing in the panel was $p_2 = 85$ mm. The outer diameter of the superheater tubes was $d_{out} = 2r_{out} = 42.4$ mm, and the inner diameter was $d_{in} = 2r_{in} = 29.8$ mm. The average tube length in each superheater pass was $L = 20.085$ m. The length L was calculated by dividing the total length of all tubes in the panel by $12 \times 4 = 48$.

In the thermal–fluid calculations of the superheater, it was assumed that the length of the tubes in each superheater pass was the same. The equivalent length of a single pass was determined by dividing the total length of all tubes in the superheater by the number of parallel tubes in the superheater equal to $12 \times 88 = 1056$.

The flow arrangement of the superheater under consideration with division into finite volumes is depicted in Figure 4. Each superheater tube was divided into n finite volumes. The superheater calculations were carried out for the given mass flow rates of steam $\dot{m}_w$ and flue gas $\dot{m}_a$. At the superheater inlet, the pressure $p_{w4,1} = p'_w$ and the steam temperature $T_{w4,1} = T'_w$ were known. The flue gas temperature at the superheater inlet was uniform and was T'_a, i.e., $T_{a1,i} = T'_a$ for $i = 1, \ldots, n$. The calculation of the steam temperature started with the outlet from the first row of tubes as the heat exchanger was cross-flow-counter.

The following designations are used in Figure 4: $T_{a1,i}$—flue gas temperature at the i-th node upstream of the first tube row; $T_{a2,i}$, $T_{a3,i}$, $T_{a4,i}$, and $T_{a5,i}$—flue gas temperature downstream of the first, second, third, and fourth row of tubes, respectively; $T_{w1,i}$, $T_{w2,i}$, $T_{w3,i}$, and $T_{w4,i}$—the steam temperature at the i-th node of the first, second, third, and fourth row of tubes, respectively.

The calculation of the superheater shown in Figure 4 can be carried out in two different ways depending on the data available. If the outlet temperature of the steam $T_{w1,n+1} = T''_w$ is known, it is possible to step in the opposite direction of the steam flow by calculating the temperatures $T_{w1,i}$ for $i = n, \ldots, 1$ first. Then, the steam temperature at the outlet of the second tube row is known from the first tube row calculation, i.e., the following condition is assumed for the calculation $T_{w2,n+1} = T_{w1,1}$. The steam temperatures $T_{w2,i}$ at the nodes $i = n, \ldots, 1$ are calculated sequentially by stepping from the right side of the superheater to the left. In the third row of pipes, it is assumed that $T_{w3,n+1} = T_{w2,1}$, where the temperature $T_{w2,1}$ was obtained from the calculations of the second tube row. For the fourth pass, the following boundary condition is assumed: $T_{w4,n+1} = T_{w3,1}$. By calculating the temperatures at nodes successively, $i = n, \ldots, 1$, one finds the steam temperature $T_{w4,1}$ at the superheater inlet. The HTC on the flue gas side is determined from the condition of equality of the calculated $T^{calc}_{w1,n+1}$ and measured $T^{meas}_{w1,n+1}$ steam temperature at the superheater outlet, i.e., from the condition $T^{calc}_{w1,n+1} = T^{meas}_{w1,n+1}$. The $T^{calc}_{w1,n+1}$ temperature can be determined at each iterative step from the expression for heat exchanger efficiency P_a for a given HTC h_a on the flue gas side. The P-NTU method was used to determine the efficiency of the P_a superheater. The P_a efficiency was determined using the formula given in [30].

In the second case, when the steam temperature $T_{w1,n+1}$ at the superheater outlet is not known, the determination of the steam temperature $T_{w4,1}$ at the superheater inlet proceeds as follows. First, the HTC h_a on the flue gas side is calculated. The formulae given in the standard method [19] can be used to calculate the HTC. Formulae given in [19] take into account the radiation [19,21] and convection [18] components of the HTC. The determination of the $T_{w4,1}$ steam temperature is carried out iteratively. The temperature $T_{w1,n+1}$ is chosen so that the temperature $T^{calc}_{w4,1}$ calculated by the proposed method and the set temperature $T^{set}_{w4,1}$ are equal to each other. The symbol $T^{set}_{w4,1}$ denotes the design or measured steam temperature at the superheater inlet.

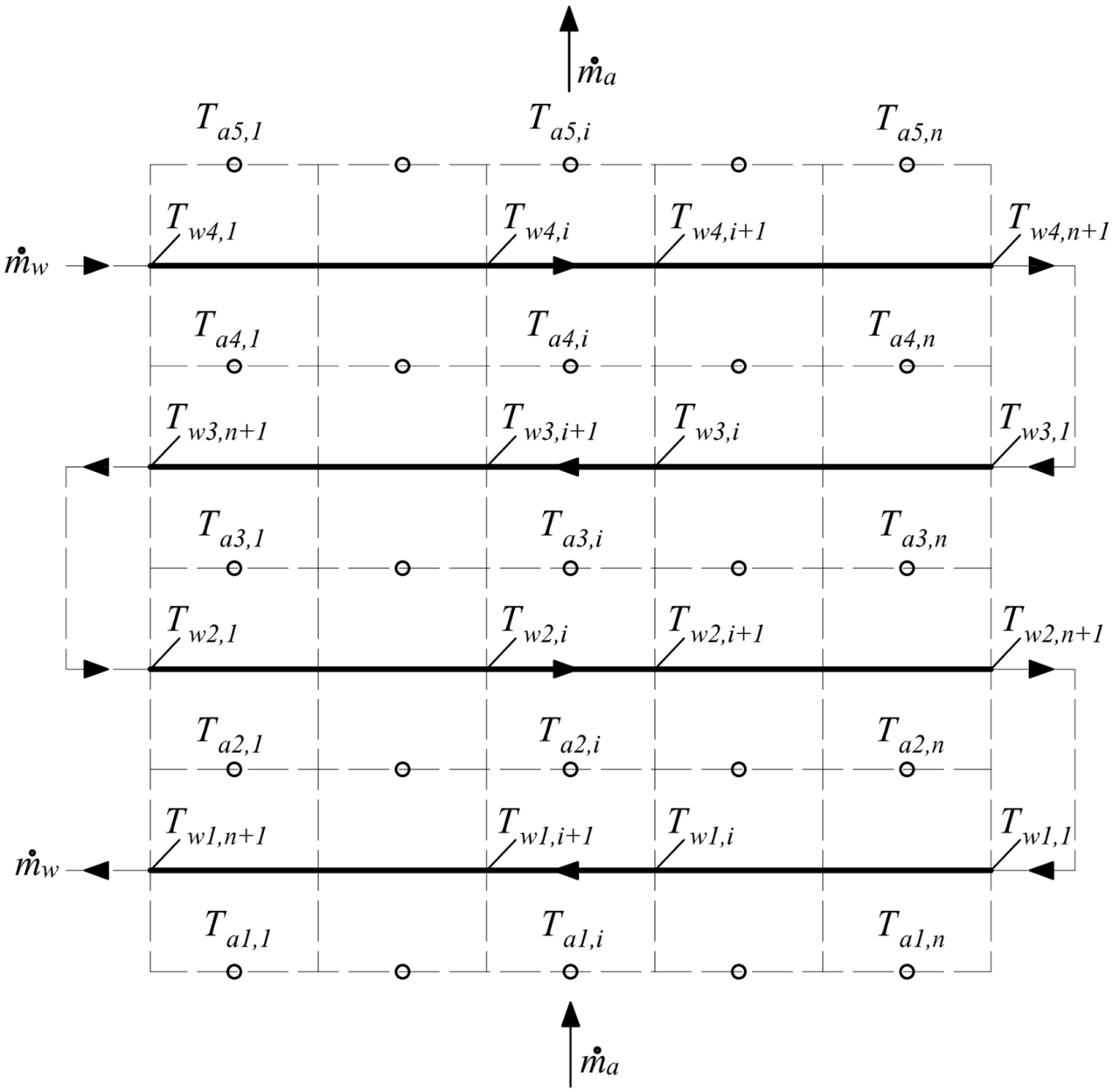

Figure 4. The layout of the superheater under consideration with division into finite volumes.

Calculations of steam temperature, flue gas temperature, tube wall temperature, and steam pressure were carried out with a single superheater pass divided into $n = 10$ finite volumes. The physical properties of the steam were calculated using the equations given in the ASME steam tables [30] and by Wagner and Kretzschmar [31]. The equations given by Brandt [32] were used to calculate the flue gas properties as a function of temperature. An in-house calculation programme in FORTRAN 90 was developed for the flow–thermal calculations of the superheater under analysis.

The boiler burned hard coal with the following mass proportions of the individual components: C = 52.6%, H_2O = 20.8%, H_2 = 3.64%, S = 0.9%, and N_2 = 0.79%. The mass flow rate of hard coal was $\dot{m}_f = 92.94$ kg/s, and the excess air number at the combustion chamber outlet was equal to $n_{air} = 1.407$. The calculated and measured flue gas flow rates were equal: $\dot{m}_a^{\mathrm{sup}} = 999.4$ kg/s. The steam and flue gas temperatures determined during measurements carried out at full load of the $\dot{m}_w^{\mathrm{sup}} = 637.12$ kg/s boiler were as follows: the steam temperature at the superheater inlet $T_{w4,1} = 465.6$ °C, the steam temperature

at the superheater outlet $T_{w1,n+1} = 526.83$ °C, average flue gas temperature before the superheater $T'_a = 731.65$ °C, and average flue gas temperature after the superheater $T''_a = 596.57$ °C. The steam pressures at the inlet and outlet of the superheater were equal to $p_{in} = 29.6025$ MPa and $p_{out} = 29.2175$ MPa, respectively. The absolute roughness was assumed to be $R_a = 0.45$ mm. The thermal conductivity of the tube material was equal to 25.76 W/(m·K). The HTC at the inner surface of the tubes calculated from Equation (13) was $h_w = 4586.5\ \mathrm{W/(m^2 \cdot K)}$. The HTC on the flue gas side was determined from the experimental data presented above so that the superheater effectiveness was equal to the effectiveness calculated using the measured steam and flue gas temperatures.

The pre-selected value of the HTC h_w using the P-NTU method was improved using the proposed numerical superheater model. The value of h_w was adjusted so that the steam temperature calculated and measured at the outlet of the superheater were equal to each other.

The effectiveness of the four-pass steam superheater shown in Figure 3 can be calculated, assuming constant physical properties of the steam and flue gas, using the following formula given by Thulukkanam [33] and by Nicole [34]:

$$P_a = \frac{\overline{T}'_a - \overline{T}''_a}{\overline{T}'_a - T'_w} \tag{24}$$

where the steam inlet temperature is $T'_w = T_{w4,1}$ (Figure 4). The symbols $\overline{T}'_a$ and $\overline{T}''_a$ designate the mean flue gas temperature before and after the superheater. The thermal efficiency of the superheater on the flue gas side is given by the formula [25,26]:

$$P_a = \frac{1}{C^*}\left(1 - \frac{1}{\zeta_e}\right) \tag{25}$$

where C^* is defined as follows:

$$C^* = \frac{\dot{m}_a\ \bar{c}_{pa}}{\dot{m}_w\ \bar{c}_{pw}} = \frac{\mathrm{NTU}_w}{\mathrm{NTU}_a} \tag{26}$$

The symbol ζ_e in Formula (25) denotes the following expression:

$$\zeta_e = \frac{K}{2}\left(1 - \frac{K}{2} + \frac{K^2}{4}\right) + K\left(1 - \frac{K}{2}\right)\left[1 - \frac{C^*}{8}K\left(1 - \frac{K}{2}\right)e^{2KC^*}\right] + e^{4KC^*}\left(1 - \frac{K}{2}\right)^3 \tag{27}$$

where K is calculated from the following relationship:

$$K = 1 - \exp\left(-\frac{\mathrm{NTU}_a}{4}\right) \tag{28}$$

The HTC on the flue gas side h_a determined from the equality condition of the superheater efficiency was calculated using the Formula (24), and the efficiency determined from experimental data was $h_a = 98.8\ \mathrm{W/(m^2 \cdot K)}$.

The results of the superheater calculations (Figure 4) are shown in Figures 5 and 6.

It can be seen (Figure 5) that the highest steam temperature occurred in the first tube row (fourth pass) and the lowest in the fourth tube row (first pass). The average temperature differences between the outer surface of the tube and the steam along the length of the individual tube rows were $\Delta T^I_{w,t} = 10.81$ K in the first tube row, $\Delta T^{II}_{w,t} = 9.69$ K in the second tube row, $\Delta T^{III}_{w,t} = 8.60$ K in the third tube row, and $\Delta T^{IV}_{w,t} = 7.55$ K in the fourth tube row. The temperature difference between the outer surface of the tube and the steam decreases in successive tube rows as the highest temperature difference between the flue gas and steam occurred in the first tube row and the lowest in the fourth tube row. The average temperature differences between the flue gas and the outer surface of the tube along the length of the individual tube rows were $\Delta T^I_{a,t} = 184.00$ K in the first

tube row, $\Delta T_{a,t}^{II} = 163.24$ K in the second tube row, $\Delta T_{a,t}^{III} = 146.13$ K in the third tube row, and $\Delta T_{a,t}^{IV} = 127.31$ K in the fourth tube row. The differences between the flue gas temperature and the tube wall temperature in the individual tube rows were much greater than the respective differences between the wall and steam temperatures. This is due to the significantly higher heat transfer coefficient on the steam side's inner tube surfaces than on the outer tube surface on the flue gas side. This also reduced the heat flux at the outer surface of the tubes, which was transferred from the flue gas to the steam. The heat fluxes on the individual tube rows were $\dot{q}^{I}(r_{out}) = 18011.24$ W/m^2 in the first tube row, $\dot{q}^{II}(r_{out}) = 16140.47$ W/m^2 in the second tube row, $\dot{q}^{III}(r_{out}) = 14315.40$ W/m^2 in the third tube row, and $\dot{q}^{IV}(r_{out}) = 12578.96$ W/m^2 in the fourth tube row.

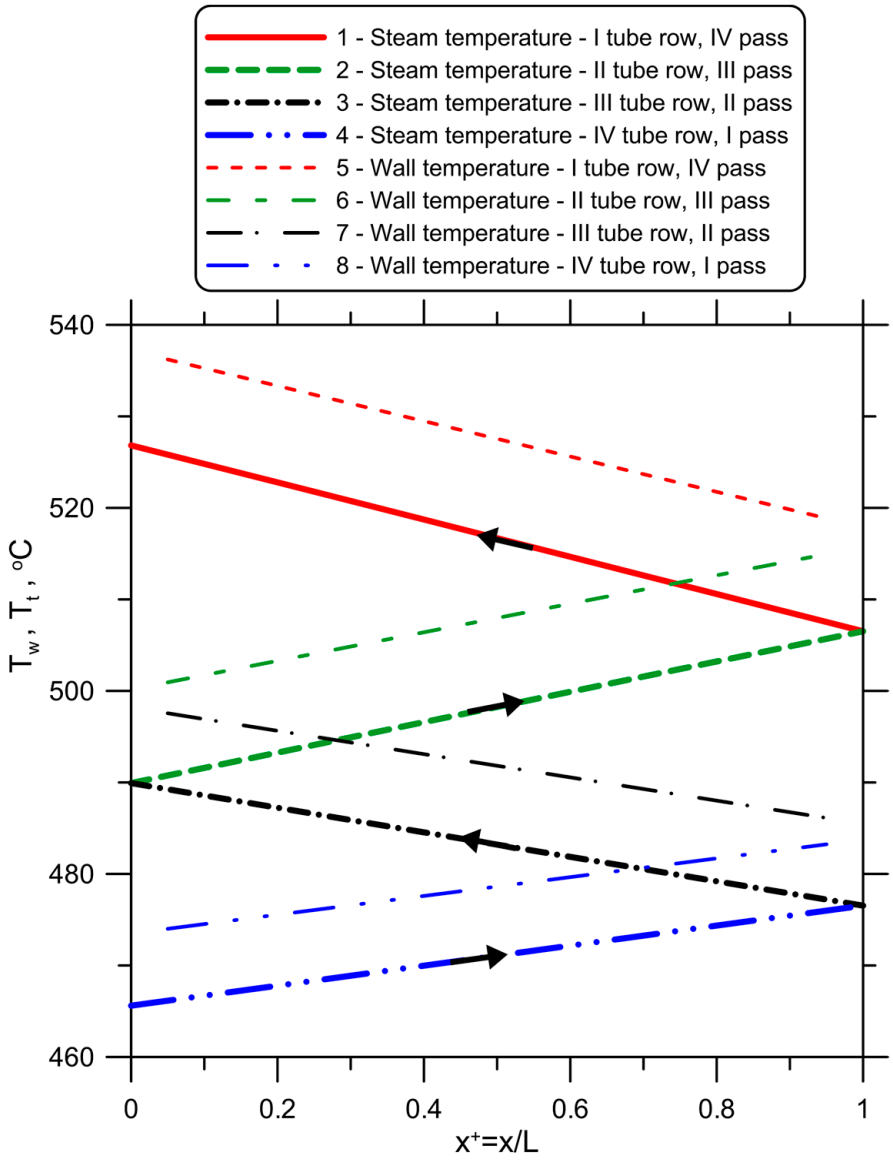

Figure 5. Variations in steam temperature $T_w(x^+)$ and the outer surface of tubes $T_t(x^+,\ r_{out})$ along the superheater length; arrows on the curves indicate the direction of steam flow.

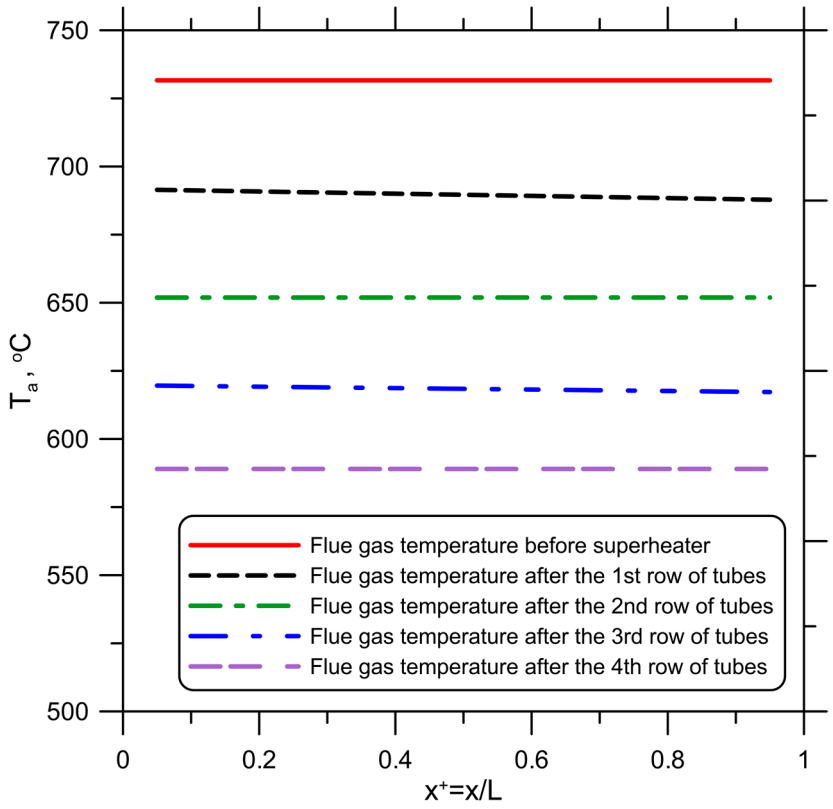

Figure 6. Temperature distribution $T_a(x^+)$ of the flue gases over the superheater length.

The heat flux values were calculated at the centre of the tube length. The calculated and measured steam temperature at the outlet of the first tube row (fourth pass) was $T_{w1,n+1} = 526.83$ °C. The temperatures were the same because the steam temperature at the outlet of the first tube row was taken as the input for the calculation. The calculated steam temperature at the superheater inlet $T_{w4,1} = 465.6$ °C was equal to the measured value.

Figure 6 shows the flue gas temperature distributions along the length of the superheater downstream of the individual tube rows. From an analysis of the results shown in Figure 6, it can be seen that the flue gas temperatures behind the different tube rows varied a little over the width of the superheater. The differences in flue gas temperature at points $x^+ = 0.05$ and $x^+ = 0.95$ behind the individual tube rows were minor: 3.46 K, (−0.03) K, 2.30 K, and (−0.04) K behind the first, second, third and fourth rows of tubes, respectively. In the calculations, the measured flue gas temperature of 731.65 °C was used as the flue gas temperature at the superheater inlet. The average flue gas temperature after the superheater calculated using the proposed method was $\overline{T}''_a = 592.09$ °C, while the measured temperature was 596.57 °C.

The heat flow rate $\dot{Q}_a$ transferred in the superheater from the flue gas to the steam and the heat flow rate $\dot{Q}_w$ taken up in the superheater by the steam were then compared to assess the accuracy of the developed model. To further assess the validity of the developed mathematical model of the superheater, the average outlet temperatures of the steam and flue gas were calculated using the P-NTU method. The relative difference e_T between the calculated and measured temperature difference of the flue gas behind the superheater to the measured flue gas temperature difference on the superheater was $e_T = 100\ (592.09 - 596.57)/(731.65 - 596.57) = 100(-4.48/135.08) = -3.32\%$. The heat flow rate calculated for the flue gas side was

$$\dot{Q}_a = \dot{m}_a^{\mathrm{sup}} \left(c_{pa}\big|_{0\ ^\circ\mathrm{C}}^{\overline{T}'_a} \overline{T}'_a - c_{pa}\big|_{0\ ^\circ\mathrm{C}}^{\overline{T}''_a} \overline{T}''_a \right) \left(\overline{T}'_a - \overline{T}''_a \right) = 172378.48\ \mathrm{kW} = 172.37848\ \mathrm{MW} \quad (29)$$

while the heat flow rate calculated from the steam side was

$$\dot{Q}_w = \dot{m}_w^{\text{sup}} \left(i'_w - i''_w\right) = \dot{m}_w^{\text{sup}} \left[i_w(\overline{p}_w,\ T'_w) - i_w\left(\overline{p}_w,\ T''_w\right)\right] = \\ = 637.12\ (3202.4835 - 2929.6513) = 173826.74\ \text{kW} = 173.82674\ \text{MW} \tag{30}$$

In Formulas (29) and (30), the following designations were used:
$\dot{m}_a^{\text{sup}}$, $\dot{m}_w^{\text{sup}}$—the mass flow rate of flue gas and steam through the entire superheater,
$\overline{T}'_a$, $\overline{T}''_a$—average flue gas temperature before and after the superheater.
The relative difference between $\dot{Q}_a$ and $\dot{Q}_w$ was

$$\varepsilon_{\dot{Q}} = \frac{\dot{Q}_w - \dot{Q}_a}{\dot{Q}_w}\ 100\% = \frac{173826.74 - 172378.48}{173826.74}\ 100\% = 0.83\% \tag{31}$$

The low value of the relative difference $\varepsilon_{\dot{Q}}$ demonstrates the perfect accuracy of the numerical superheater model.

The superheater outlet steam temperature and the mean flue gas temperature after the superheater were also calculated using the P-NTU method [33,34]. When calculating the P_a efficiency from Equation (25), it was considered that the average values of the number of heat transfer units were equal to NTU_w = 0.3826 and NTU_a = 0.8617 for steam and flue gas, respectively. The superheater efficiency calculated from Equation (25) was 0.5206. The average flue gas temperature after the superheater $\overline{T}''_a$ was determined using the definition of the effectiveness given by Equation (24):

$$\overline{T}''_a = \overline{T}'_a - P_a\left(\overline{T}''_a - T'_w\right) \tag{32}$$

Using Equation (32), the following value $\overline{T}''_a$ was obtained: $\overline{T}''_a = 593.16$ °C. The temperature of the steam at the superheater outlet was determined by the condition of equality of the heat flow rate transferred from the flue gas to the steam. The outlet steam temperature T''_w is given by

$$T''_w = T'_w + \frac{NTU_w}{NTU_a}\left(\overline{T}'_a - \overline{T}''_a\right) \tag{33}$$

After substituting the data into Equation (33), the following value of outlet steam temperature was obtained: $T''_w = 527.08$ °C. The values obtained for flue gas and steam temperatures downstream of the superheater agreed with the corresponding values obtained from the proposed superheater model despite assuming constant specific heat of steam and flue gas in the P-NTU method. However, the P-NTU method does not allow the determination of the tube wall temperature in each pass, which is needed when selecting the steel grade for a given pass. Due to the high cost of alloy steels, the individual superheater runs were made from different steel grades matched to the tube wall temperature in a given pass.

Figure 7 shows the variation of steam pressure in the superheater along the superheater steam flow path.

The steam pressure at the superheater inlet was $p_{w4,1} = 296.025$ bar, and at the outlet $p_{w1,n+1} = 292.175$ bar. The calculated steam pressure drop in the superheater was equal to the measured steam pressure drop $(p_{w4,1} - p_{w1,n+1}) = (296.025 - 292.175) = 3.85$ bar because the absolute surface roughness of the superheater tubes was chosen so that the calculated and measured steam outlet pressures were the same. From the analysis of the results shown in Figures 5–7, it can be seen that the developed numerical model of the four-pass counter-flow steam superheater has excellent accuracy.

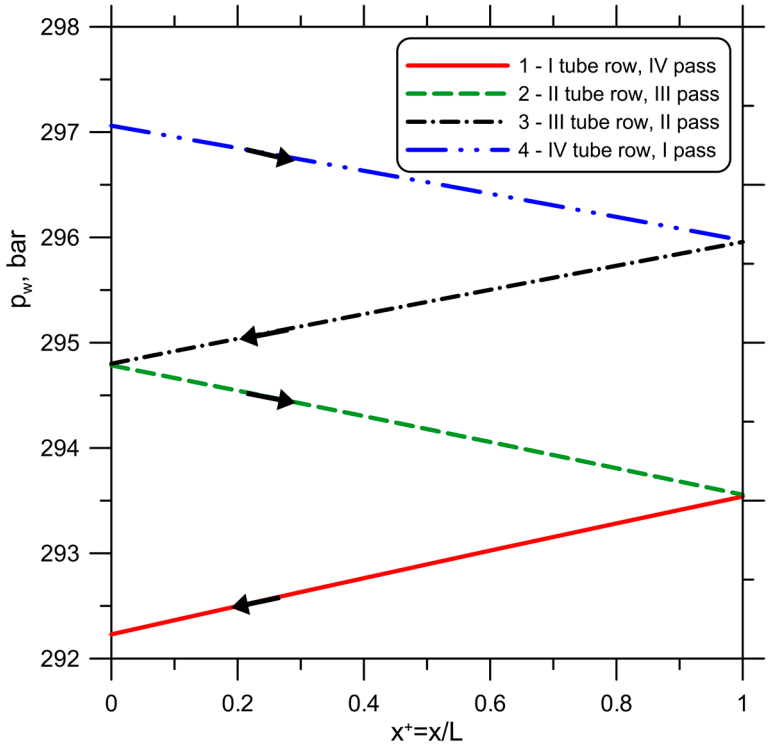

Figure 7. Steam pressure distribution over the superheater length; arrows on the curves indicate the direction of steam flow.

4. Conclusions

This paper presents a new numerical thermal–flow model of a four-pass cross-flow steam superheater installed in a supercritical boiler. The non-linear superheater model accounts for the temperature and pressure-dependent specific heat of the steam. The specific heat of the flue gas was assumed to be temperature-dependent. The accuracy of the calculations is already satisfactory, even with a number of finite volumes along the length of one superheater pass equal to or greater than ten. The relative difference between the heat flow rate taken up by the steam and the heat flow rate given off by the flue gas is 0.83% when dividing one superheater pass into ten finite volumes. As a result of the calculations using the proposed model, the spatial distribution of steam and flue gas temperatures is obtained. By determining the wall temperature distribution along the length of the tubes in each pass, the appropriate steel grade for each pass can be selected. This can reduce superheater construction costs while avoiding overheating the tube material. It is worth mentioning that overheating of the tube material is the main cause of superheater tube failure. The superheater modelling method used in this study can be easily applied to superheaters' performance and design calculations. The numerical model of the superheater can easily be extended to account for the unevenness of the flue gas temperature in front of the superheater. Application of the developed method is straightforward, including subcritical and supercritical superheaters with a large number of passes and tube rows. Similar models can be developed for all superheater stages in a boiler and used in a computer boiler monitoring system. Such a monitoring system can be used to operate the boiler with high efficiency while maintaining a long superheater life. In future studies, the superheater model presented in this paper can be extended to consider scales on the tube's inner surfaces and ash fouling on the tube's outer surfaces. The proposed modelling of superheaters can be extended to include the uneven distribution of flue gas temperature across the flue duct cross-section and the different mass flow rates of steam through the individual panels.

Author Contributions: Conceptualization, K.W.; methodology, software, validation, formal analysis, investigation, writing—original draft preparation, K.W. and D.T.; resources, data curation, J.T. and M.M.; writing—review and editing, supervision, K.W., D.T. and J.T. All authors have read and agreed to the published version of the manuscript.

Funding: This work was supported by the National Centre for Research and Development Programme "Small Grant Scheme 2020" implemented under The Norwegian Financial Mechanism 2014–2021: [grant number NOR/SGS/MECHEX/0080/2020].

Data Availability Statement: Not applicable.

Conflicts of Interest: The authors declare no conflict of interest.

Nomenclature

Latin symbols

A	cross-section area of the duct, m^2
$c_{pa,i}$	specific heat capacity of the flue gas at the temperature T_i, J/(kg·K)
$\overline{c}_{pa,\,i}$	average specific heat capacity of the flue gas at the i-th finite volume, J/(kg·K)
$c_{pw,i}$	specific heat capacity of the steam at the temperature T_i, J/(kg·K)
$\overline{c}_{pw,i}$	average specific heat capacity of the steam at the i-th finite volume, J/(kg·K)
C^*	the ratio of the heat capacity rates of the flue gas and steam
d_{in}	inner tube diameter, m
d_{out}	outer tube diameter, m
d_h	hydraulic diameter, m
e_T	relative difference between the calculated and measured temperature difference of the flue gas after the superheater to the measured flue gas temperature difference on the superheater, %
g	gravitational acceleration, m/s^2
h_a	heat transfer coefficient on the outer tube surface, $W/(m^2 \cdot K)$
h_w	heat transfer coefficient on the tube inner surface, $W/(m^2 \cdot K)$
$h^j_{w,i}$	heat transfer coefficient on the tube inner surface at the node i, $W/(m^2 \cdot K)$
$h^j_{a,i}$	heat transfer coefficient on the tube outer surface at the node i, $W/(m^2 \cdot K)$
k_i	overall heat transfer coefficient at the i-th finite volume, $W/(m^2 \cdot K)$
L_x	tube length, m
$\dot{m}_a$	the mass flow rate of the flue gas, kg/s
$\dot{m}_{a,i}$	the mass flow rate of gas through the i-th finite volume, kg/s
$\dot{m}_f$	the mass flow rate of hard coal, kg/s
$\dot{m}_w$	the mass flow rate of the steam, kg/s
n_{air}	the excess air number at the outlet of the combustion chamber
n_t	number of tube rows in the heat exchanger
p_1	the transverse tube spacing, m
p_2	the longitudinal tube spacing, m
P_a	the thermal effectiveness of the superheater on the flue gas side
p_{in}	the steam inlet pressure, Pa
p_{out}	the steam outlet pressure, Pa
p_w	static pressure of the steam, Pa
$\dot{Q}_a$	the heat flow rate from the flue gas, W
$\dot{Q}_w$	the heat flow rate taken up by the steam, W
$\dot{q}^j_{out,i}$	heat flux at the outer surface of the tube for the i-th finite volume and j-th tube row, W/m^2
R_a	absolute roughness of the inner tube surface, m
r_{in}	tube inner radius, m
r_{out}	tube outer radius, m
s	the coordinate passing through the centre of gravity of the duct cross-section, with the same direction as that of the velocity vector, m
T'_a	flue gas temperature in front of the tube row, °C
T''_a	flue gas temperature after the tube row of, °C

$T^{j}_{t,i}(r_{out})$	the temperature of the tube outer surface in the *i*-th finite volume in the *j*-th row, °C
$T_{w,i}$	steam inlet temperature to the *i*-th finite volume, °C
$T_{w,i+1}$	steam outlet temperature from the *i*-th finite volume, °C
$\overline{T}^{j}_{w,i}$	mean temperature of the steam over the finite volume length Δx_i, °C
w	steam velocity, m/s
x_i , x_{i+1}	node coordinate at the inlet and outlet of the finite volume, m
Greek symbols	
$\Delta A_{out,i}$	the outer surface area of a bare tube within one finite volume, m^2
$\Delta \dot{m}_{a,i}$	the mass flow rate of the flue gas through *i*-th finite volume, kg/s
$\Delta N_{a,i}$	the number of transfer units for flue gas for *i*-th finite volume
$\Delta N_{w,i}$	the number of transfer units for steam for *i*-th finite volume
Δx_i, Δy	dimensions of finite volume, m
ε	relative roughness, R_a/r_{in}
$\varepsilon_{\dot{Q}}$	the relative difference between the heat flow rate $\dot{Q}_w$ absorbed by the steam and the flow rate $\dot{Q}_a$ given off by the flue gas
ρ	density, kg/m^3
φ	angle of the tube to the horizontal, rad
ξ	Darcy–Weisbach friction factor
λ^{j}_{i}	tube thermal conductivity for *i*-th finite volume in *j*-th tube row, W/(m·K)
ζ_j	pressure loss coefficient for 90º bend
Subscripts	
a	flue gas
i	node number
w	steam
Superscripts	
calc	calculated
j	number of tube row
meas	measured
sup	superheater
Abbreviations	
3D	three-dimensional
CFB	circulating fluidised bed boiler
CFD	computational fluid dynamics
HTC	heat transfer coefficient
LMTD	logarithmic mean temperature difference
NTU	number of heat transfer units
P1	the method of spherical harmonics for radiation heat transfer

References

1. French, D.N. *Metallurgical Failures in Fossil Fired Boilers*, 2nd ed.; John Wiley & Sons: Hoboken, NJ, USA, 1993.
2. Pronobis, M. *Environmentally—Oriented Modernisation of Power Boilers*; Elsevier: Amsterdam, The Netherlands, 2020.
3. Omar, M.; Ashraf, K.; Wang, J. Modeling and Control of Supercritical and Ultra-Supercritical Power Plants: A Review. *Energies* **2020**, *13*, 2935. [CrossRef]
4. Hedrick, K.; Hedrick, E.; Omell, B.; Zitney, S.E.; Bhattacharyya, D. Dynamic Modeling, Parameter Estimation, and Data Reconciliation of a Supercritical Pulverized Coal-Fired Boiler. *Ind. Eng. Chem. Res.* **2022**, *61*, 16764–16779. [CrossRef]
5. Haddad, A.; Mohamed, O. Qualitative and quantitative comparison of three modeling approaches for a supercritical once-through generation unit. *Int. J. Energ. Res.* **2022**, *46*, 20780–20800. [CrossRef]
6. Yang, D.; Chen, L.; Chen, J.; Feng, Y. High-heat flux flow and heat transfer transitions in a supercritical loop: Numerical verification and correlation. *Int. J. Energ. Res.* **2022**, *46*, 16375–16393. [CrossRef]
7. Sun, L.; Yan, W. Prediction of wall temperature and oxide scale thickness of ferritic-martensitic steel superheater tubes. *Appl. Therm. Eng.* **2018**, *134*, 171–181. [CrossRef]
8. Li, P.; Bao, T.; Guan, J.; Shi, Z.; Xie, Z.; Zhou, Y.; Zhong, W. Computational Analysis of Tube Wall Temperature of Superheater in 1000 MW Ultra-Supercritical Boiler Based on the Inlet Thermal Deviation. *Energies* **2023**, *16*, 1539. [CrossRef]
9. Qi, J.; Zhou, K.; Huang, J.; Si, X. Influence of temperature on the oxide spallation of T91 alloy superheater tubes in power plant. *Appl. Therm. Eng.* **2018**, *128*, 244–252. [CrossRef]
10. Balint, R.; Engblom, M.; Niemi, J.; Silva da Costa, D.; Lindberg, D.; Yrjas, P.; Hupa, L.; Hupa, M. Temperature gradient induced changes within superheater ash deposits high in chlorine. *Energy* **2021**, *226*, 120439. [CrossRef]
11. Liu, W. A superheater creep-fatigue interaction failure and its stress assessment. *Eng. Fail. Anal.* **2021**, *119*, 105004. [CrossRef]

12. Ma, Y.; Jin, X.; Lyu, J. Analysis of thermal deviations in L-shape platen superheaters of a supercritical 600 MW circulating fluidised bed boiler. *Appl. Therm. Eng.* **2020**, *166*, 114752. [CrossRef]
13. Hossain, M.N.; Ghosh, K.; Manna, N.K. Integrated thermal modeling, analysis, and sequential design of heat exchanger surfaces of a natural circulation RDF boiler including evaporator tubes. *Appl. Therm. Eng.* **2022**, *211*, 118455. [CrossRef]
14. Yao, Y.; Cai, R.; Zhang, Y.; Zhang, M.; Yang, H.; Lyu, J. A method to measure the tube-wall temperature in CFB boilers. *Appl. Therm. Eng.* **2019**, *153*, 493–500. [CrossRef]
15. Laubscher, R.; Rousseau, P. Coupled simulation and validation of a utility-scale pulverised coal-fired boiler radiant final-stage superheater. *Therm. Sci. Eng. Prog.* **2020**, *18*, 100512. [CrossRef]
16. Granda, M.; Trojan, M.; Taler, D. CFD analysis of steam superheater operation in steady and transient state. *Energy* **2020**, *199*, 117423. [CrossRef]
17. Madejski, P.; Taler, D.; Taler, J. Thermal and flow calculations of platen superheater in large scale CFB boiler. *Energy* **2022**, *258*, 124841. [CrossRef]
18. Lokshin, V.A.; Peterson, D.F.; Schwarz, A.L.; Sheehan, M.E. *Standard Methods of Hydraulic Design for Power Boilers*; Springer: Berlin/Heidelberg, Germany, 1988.
19. Kagan, G.M. *Thermal Calculation of Boilers (Normative Method)*, 3rd ed.; Revised and Expanded; All-Russia Thermal Engineering Institute: St. Petersburg, Russia, 1998. (In Russian)
20. Olenev, E.A. Method of analytical calculation radiating (steam) superheater of the steam locomotive. *IFAC Proc. Vol.* **2009**, *42*, 1708–1713. [CrossRef]
21. Taler, D.; Taler, J. Simplified analysis of radiation heat exchange in boiler superheaters. *Heat Transfer Eng.* **2009**, *30*, 661–669. [CrossRef]
22. Taler, D.; Taler, J.; Wrona, K. New analytical-numerical method for modeling of tube cross-flow heat exchangers with complex flow systems. *Energy* **2020**, *228*, 120633. [CrossRef]
23. Węglarz, K.; Taler, D.; Taler, J. New non-iterative method for computation of tubular cross-flow heat exchangers. *Energy* **2022**, *260*, 124955. [CrossRef]
24. Taler, D. Simple power-type heat transfer correlations for turbulent pipe flow in tubes. *J. Therm. Sci.* **2017**, *26*, 339–348. [CrossRef]
25. Taler, D.; Taler, J. Simple heat transfer correlations for turbulent tube flow. *E3S Web Cof.* **2017**, *13*, 2008. [CrossRef]
26. Taler, D. *Numerical Modelling and Experimental Testing of Heat Exchangers*; Springer: Cham, Switzerland, 2019.
27. Idelchik, I.E. *Handbook of Hydraulic Resistance*, 4th ed.; Begell House, Inc. Publishers: Redding, CA, USA, 2021.
28. Moody, L.F. Friction factors for pipe flow. *Trans. Am. Soc. Mech. Eng.* **1944**, *66*, 671–684. [CrossRef]
29. Rennels, D.C.; Hudson, H.M. *Pipe flow. A Practical and Comprehensive Guide*, 2nd ed.; AIChE, Wiley: Hoboken, NJ, USA, 2020.
30. Meyer, C.A. *ASME Steam Tables-Thermodynamic and Transport Properties of Steam*, 6th ed.; ASME: New York, NY, USA, 1993.
31. Wagner, W.; Kretzschmar, H.-J. *International Steam Tables. Properties of Water and Steam Based on the Industrial Formulation IAPWS-IF97*, 2nd ed.; Springer: Berlin/Heidelberg, Germany, 2008.
32. Brandt, F. *Wärmeübertragung in Dampferzeugern und Wärmeaustauschern*; Vulkan-Verlag: Essen, Germany, 1995.
33. Thulukkanam, K. *Heat Exchanger Design Handbook*, 2nd ed.; CRC Press—Taylor & Francis Inc.: Boca Raton, FL, USA, 2013.
34. Roetzel, W.; Nicole, F.J.L. Mean temperature difference for heat exchanger design. *J. Heat Transfer.* **1975**, *97*, 5–8. [CrossRef]